



ELSEVIER

Computational Materials Science 15 (1999) 302–310

COMPUTATIONAL  
MATERIALS  
SCIENCE

# Modeling the anode boundary layer of high-intensity argon arcs

C.S. Wu<sup>a,\*</sup>, M. Ushio<sup>b</sup>, M. Tanaka<sup>b</sup><sup>a</sup> Institute of Joining Technology, Shandong University of Technology, 73 Jingshi Road, Jinan 250061, People's Republic of China<sup>b</sup> Welding Research Institute, Osaka University, Osaka, Japan

Received 22 February 1999; accepted 7 April 1999

## Abstract

This paper is concerned with numerical studies of the anode region of a high-intensity argon arc. The anode region is divided into three subzones: the anode boundary layer, the presheath and the sheath. The governing equations of the dominating processes with the boundary conditions taken from the solutions of LTE plasmas are solved by applying the Runge–Kutta procedure. One parameter  $\theta$ , i.e., the ratio of the heavy particle temperatures at the free-fall edge to the anode surface temperatures, is introduced into this study. The results indicate that the parameter  $\theta$  is an important factor influencing the local plasma properties in the boundary layer, the boundary layer thickness and the sheath potential. An estimate of the value for  $\theta$  is made. The potential drop in the boundary layer is slightly positive. © 1999 Elsevier Science B.V. All rights reserved.

*Keywords:* Modeling; Anode boundary layer; Argon arc

## 1. Introduction

Thermal plasmas have a number of applications in material and chemical processing, such as welding, cutting, spraying, chemical vapor deposition, physical vapor deposition, sintering and material melting. The primary method for producing thermal plasmas employs a high-intensity arc which is defined as a discharge operated at current levels above 50 A and pressures above 10 kPa [1]. High-intensity arcs are characterized by strong macroscopic flows induced by the arc itself. At the cathode, electrons are thermally emitted

from a small, hot region known as the cathode spot. From the cathode spot the electrons diverge radially and move axially toward the anode. The strong divergence of the current at the cathode gives rise to significant electromagnetic forces which drive the cathode jet, a high-speed flow of gas, toward the anode. As the cathode jet impinges on the anode, a stagnation layer is formed in front of the anode, resulting in the well-known bell shape of free-burning, high-intensity arcs [2]. In general, such an arc may be divided into a flow-affected region which represents the main body of the arc (arc column), an anode region, and a cathode region. In spite of extensive efforts in the arc physics and arc technology [3–7], the understanding of the arc behavior still remains incomplete. Especially, there is still a lack of basic understanding of the arc electrode regions of

\* Corresponding author. Present address: University of Hannover, Joining of Materials, Applestr. 11A, 30167 Hannover, Germany. E-mail: wu@iw.uni-hannover.de

high-intensity arcs and of the associated electrode phenomena. The proximity of the electrode gives rise to extremely steep gradients of the plasma properties which render experimentation even more difficult in this generally hostile environment. Achieving an effective utilization and exploitation of high-intensity arcs requires a through understanding of the plasma properties and its physical processes in the proximity of the anode surface.

This paper is concerned with the anode region of high-intensity arcs, operated in Argon atmosphere with plane, water-cooled Cu anode. The anode region is generally defined as that part of the arc discharge which contains the surface of the anode, the sheath in front of the anode and the boundary layer which makes the connection to the arc column [8]. Although there has been some research of the anode region of electric arcs over the past years, a consistent theory is still lacking which would, for example, predict the sign and the magnitude of the anode fall in high-intensity arcs. According to the analysis of [9], the electric field strength in the anode boundary layer should be less than that in the adjacent arc column; but the anode fall should still be positive for high-intensity arcs. Bose [10] presented a one-dimensional analysis of the wall region for an argon plasma. The electric current may flow into or from the wall in the normal direction (wall as anode or cathode). He found that the anode potential is slightly negative. Dinulescu and Pfender [11] carried out an analysis of the anode boundary layer, which predicts negative anode falls. Their results show that the electric field, starting from a small positive value at the arc column side, turns negative inside the boundary layer and assumes large negative value in the vicinity of the anode. However, they admitted in their paper that there is a major difference in the choice of the boundary condition for solving the conservation equations for the anode boundary layer between [9] and their own work [11]. They selected much steeper temperature gradients of the plasma species as boundary conditions and assumed the heavy particle temperature decreases from the value in the plasma to 400 K which is the temperature of the anode surface. Although the water-cooled anode temperature is lower, and electron and heavy particle tempera-

tures separate in the anode boundary layer, it is justified in questioning whether or not the heavy particle temperature is equal to that of the anode surface because determining the temperature of ions close to the anode is a problem that still remains unsolved [12,13]. Furthermore, they did not make a difference between an anode surface which conducts electricity and a cool wall which is isolated (no net current flow). In their analysis, the equation determining the potential drop across the sheath gives a very large negative value for the current density range of practical interest. Therefore, greater efforts should be made continuously to achieve better understanding in this field of fundamental importance.

In this paper, solutions of the governing equations of the dominating processes are presented for the anode region. The boundary conditions at some place lying in the arc column and near the boundary layer are taken from the solutions of the flow-affected region. The analysis applies to free-burning, high-intensity arcs in argon at atmospheric pressure.

## 2. Anode boundary layer

As shown in Fig. 1, the anode region is divided into three subzones: the anode boundary layer, the presheath and the sheath. In the boundary layer, the presence of the relatively cold anode is felt. The boundary layer is characterized by steep gradients of temperature and particle densities. The bound-

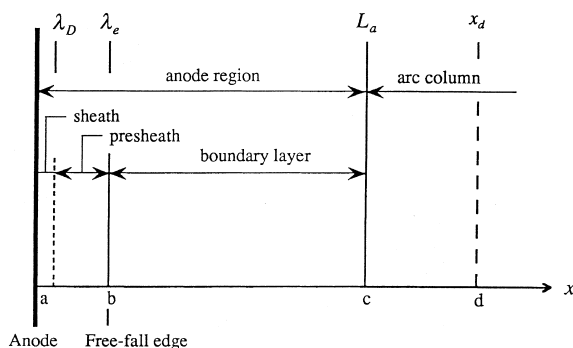


Fig. 1. Schematic sketch of the computational domain.

dary layer thickness is in the order of  $10^{-1}$  mm which is much larger than the particle mean-free-path length. The main feature of the boundary layer is the ionized gas in the layer may be treated as a continuum and as a true plasma. Very close to the anode (in the order of one electron mean-free-path), the usual continuum approach is no longer valid. The ionized gas in the presheath and in the sheath may not be treated as a continuum because the total thickness of the presheath and the sheath is equal to one electron mean-free-path. In the presheath, the neutrality of the plasma is maintained. In the Debye sheath, the neutrality is broken and sharp potential drop occurs. The sheath is formed immediately in front of the anode accommodating the transition from electrical conduction in the plasma to metallic conduction in the anode. The thickness of the sheath is in the order of the Debye length.

### 2.1. Governing equations

Due to its small thickness, the anode region may be treated as a one-dimensional region. For the purpose of solving the conservation equations, the plasma parameters are assumed to vary only in the direction perpendicular to the anode surface. In the boundary layer, the continuum approach and the condition of charge neutrality are valid. Since the electron temperature ( $T_e$ ) may be higher than the heavy particles (atoms and ions) temperature ( $T_i$ ), electrons and heavy particles are regarded as two separate fluids coexisting in the plasma.

In a three-component system (electrons, atoms and ions), the electron flux may be written as [14]

$$\vec{\Gamma}_e = n_e \vec{U}_e = -\mu_e n_e \vec{E} - \frac{\mu_e k_B T_e}{e} \nabla n_e - \frac{\mu_e k_B n_e}{e} \nabla T_e, \quad (1)$$

where  $n_e$  is the electron number density,  $\vec{U}_e$  the electron drift velocity,  $\mu_e$  the electron mobility,  $\vec{E}$  the electric field strength,  $k_B$  the Boltzmann constant and  $e$  the elementary charge. The electron flux is driven by the potential gradient ( $\vec{E} = -\nabla\phi$ ), the electron density gradient and the electron temperature gradient.

The ion flux may be expressed by

$$\vec{\Gamma}_i = n_i \vec{U}_i = \mu_i n_e \vec{E} - \frac{\mu_i k_B T_h}{e} \nabla n_e - \frac{\mu_i k_B n_e}{e} \nabla T_h, \quad (2)$$

where  $n_i$  is the ion number density,  $\vec{U}_i$  the ion drift velocity and  $\mu_i$  the ion mobility. The condition of charge neutrality is valid in the boundary layer, thus there is the relation  $n_e \approx n_i$ . The forces driving the ion flux are the potential gradient, the ion density gradient and the ion temperature gradient.

In a steady state situation without macroscopic mass flow, the particle conservation equation of the electrons becomes

$$\nabla \cdot \vec{\Gamma}_e = \dot{n}_e, \quad (3)$$

where  $\dot{n}_e$  is the net electron production rate. Under the same conditions the particle conservation equation for the ions is

$$\nabla \cdot \vec{\Gamma}_i = \dot{n}_e. \quad (4)$$

Since electron and ion production occurs in pairs, the net ion production rate equals that of the electrons.

In a plasma, the net electron production rate is the difference between the ionization rate by electron impact and the three-body recombination rate. In terms of the recombination coefficient  $\gamma$  and species composition, the net electron production rate is given by

$$\dot{n}_e = \gamma n_a \left[ \left( \frac{n_e^2}{n_a} \right)_{\text{equil}} - \frac{n_e^2}{n_a} \right], \quad (5)$$

where  $(n_e^2/n_a)_{\text{equil}}$  is the function of  $T_e$  given by Saha equation

$$\left( \frac{n_e^2}{n_a} \right)_{\text{equil}} = \frac{2Z_i}{Z} \left( \frac{2\pi m_e k_B T_e}{h^2} \right)^{3/2} \exp \left( -\frac{\varepsilon_i}{k_B T_e} \right), \quad (6)$$

where  $Z_i$  is the partition function of ion,  $Z$  the partition function of neutral atom,  $m_e$  the mass of electron,  $h$  the Planck's constant,  $n_a$  the number density of neutral atoms and  $\varepsilon_i$  the ionization potential. The number density  $n_a$  is related to the pressure  $p$  by the expression

$$n_a = \frac{p}{k_B T_h} - n_e \left( 1 + \frac{T_e}{T_h} \right). \quad (7)$$

The current density is given by

$$\vec{J} = \vec{J}_e + \vec{J}_i, \quad (8)$$

where  $\vec{J}_e$  and  $\vec{J}_i$  represents the electron and the ion contribution, respectively. According to Eqs. (1) and (2) the current density may be expressed as

$$\vec{J}_e = -e\vec{\Gamma}_e, \quad \vec{J}_i = e\vec{\Gamma}_i. \quad (9)$$

Based on Eqs. (3) and (4), there is the following relation

$$\nabla \cdot (\vec{\Gamma}_i - \vec{\Gamma}_e) = 0, \quad \vec{\Gamma}_i - \vec{\Gamma}_e = \text{constant}. \quad (10)$$

Thus, in the boundary layer

$$\vec{J} = \vec{J}_e + \vec{J}_i = e(\vec{\Gamma}_i - \vec{\Gamma}_e) = \text{constant}. \quad (11)$$

In a steady state situation without macroscopic mass flow, the energy conservation equation of the electrons may be expressed

$$\begin{aligned} \nabla \cdot (k_e \nabla T_e) + \left( \frac{5}{2} + \frac{e\phi_d}{k_B \sigma} \right) \frac{J}{e} k_B \nabla T_e + JE \\ = \left( \frac{5}{2} k_B T_e + \varepsilon_i \right) \dot{n}_e + \frac{3m_e}{m_i} k_B (T_e - T_h) n_e \vec{v}_{ei}, \end{aligned} \quad (12)$$

where  $k_e$  the electron thermal conductivity,  $\phi_d$  the thermal diffusion coefficient of the electrons,  $\sigma$  the electrical conductivity,  $m_i$  the mass of ion and  $\vec{v}_{ei}$  the average collision frequency between electrons and ions. The terms on the left-hand side of Eq. (12) contain several energy input in the sequence, heat transfer by the pure conduction, the transport of enthalpy due to the random thermal energy of electrons and the Thomson effect, and the internal energy dissipation due to Joule heating. The first term on the right-hand side of Eq. (12) represents the energy used for the production of electrons by ionization, while the second term represents the energy losses by elastic collisions between electrons and heavy particles. Here only collisions between electrons and ions have been taken into consideration since in the anode boundary layer the collision frequency between electrons and ions is much larger than that between electrons and atoms [11].

For heavy particles, the Joule heating term due to the ion current may be neglected. The energy equation of heavy particles becomes

$$-\nabla \cdot (k_h \nabla T_h) + \frac{3m_e}{m_i} k_B (T_e - T_h) n_e \vec{v}_{ei} = 0, \quad (13)$$

where  $k_h$  is the thermal conductivity of heavy particles.

The main unknowns in the set of equations are  $n_e$ ,  $T_e$ ,  $T_h$  and  $E$ . With these key variables all other quantities of interest can be computed. There are also four main differential equations, i.e., Eqs. (3), (4), (12) and (13). The other equations are auxiliary relations.

## 2.2. Boundary conditions

In order to solve the system of equations, appropriate boundary conditions must be specified. Because the thickness of the anode boundary layer  $L_a$  is an additional unknown, the boundary conditions can not be specified at the interface between the arc column and the anode boundary layer as Dinulescu and Pfender did [11]. In this study, the boundary conditions are specified at a place lying in the arc column and taken from the solutions of the arc plasma region. The distance from this place to the anode surface is a little bigger than  $L_a$ . The differential equations are solved starting from this place and then entering the anode boundary layer soon.

As shown in Fig. 1, at  $x = x_d$ : (1) the heavy particle temperature and electron temperature are identical,  $T_e = T_h = (T)_{x_d}$ ; (2) the temperature gradients of heavy particle and electron are identical,  $dT_e/dx = dT_h/dx = (dT/dx)_{x_d}$ ; (3) the electron number density,  $n_e = (n_e)_{x_d}$ ; (4) the gradient of electron number density,  $dn_e/dx = (dn_e/dx)_{x_d}$ ; (5) the current density,  $J = (J)_{x_d}$ ; and (6) the electric field strength,  $E = (E)_{x_d}$ . Among these six parameters, electron number density and its gradient are both calculated from the Saha equation at  $(T)_{x_d}$  and from  $(dT/dx)_{x_d}$ , while others are determined by the model of arc plasma region [15].

Very close to the anode (in the order of one electron mean-free-path), the usual continuum approach is no longer valid. Thus, the calculation about the boundary layer should be stopped at the free-fall edge (point  $b$  in Fig. 1), because  $x_b = \lambda_e$ . An additional boundary condition at the free-fall edge should be specified since the thickness of the anode boundary layer  $L_a$  is unknown. The ion temperature in the vicinity of anode surface is still

a problem for further study [12,13]. Thus, an adjustable parameter is defined as

$$\theta = \frac{T_{hb}}{T_a}, \quad (14)$$

where  $T_{hb}$  is the heavy particle temperature at the free-fall edge and  $T_a$  the anode surface temperature.

### 2.3. Solution methods

The set of conservation equations, i.e., Eqs. (3), (4), (12) and (13), represents four second-order differential equations including highly nonlinear, nonequilibrium thermodynamic and transport properties. By applying the Runge–Kutta procedure, these differential equations are solved starting from boundary conditions and proceeding step by step toward the anode. The value of key variables  $n_e$ ,  $T_e$ ,  $T_h$  and  $E$  are determined in the boundary layer. For each step, the nonequilibrium composition at that particular location is determined first and then the thermodynamic and transport properties are calculated using the methods described in [16]. This procedure continues until the supplementary condition  $T_h = \theta T_a$  may be recovered and the variation of the electron number density over one electron mean-free-path reaches the same order of magnitude as the electron number density itself. At this point, the continuum approach is no longer valid. The thickness of the anode boundary layer is defined as the distance from this point to the location where the difference  $T_e - T_h$  becomes less than 10% of the electron temperature  $T_e$ . The procedure allows the determination of the boundary layer thickness in addition to the values of plasma properties.

### 3. Results and discussion

As mentioned in Section 2.2, based on the model of fluid flow and heat transfer in an argon arc plasma [15], values of  $T_e$ ,  $T_h$ ,  $dT_e/dx$ ,  $dT_h/dx$ ,  $J$  and  $E$  at a location lying in the arc column can be determined. Value of  $n_e$  and  $dn_e/dx$  can be calculated from the Saha equation at  $T_e$  and from  $dT_e/dx$ . These values are used as the boundary

conditions. For a free-burning argon arc at 150 A and 1 atmosphere pressure, the corresponding boundary conditions are specified as follows:

at  $x = x_d$ :

$$T_e = T_h = 1.26 \times 10^4 \text{ K}$$

$$\frac{dT_e}{dx} = \frac{dT_h}{dx} = 4.5 \times 10^5 \text{ K/m}$$

$$n_e = 8.82 \times 10^{23} \text{ 1/m}^3$$

$$\frac{dn_e}{dx} = 2.38 \times 10^{25} \text{ 1/m}^4$$

$$J = 3.2 \times 10^6 \text{ A/m}^2$$

$$E = 2.75 \times 10^2 \text{ V/m}.$$

Figs. 2 and 3 show the temperature distributions for heavy particles and electrons, respectively. It can be seen that the value of parameter  $\theta$ , i.e., the ratio of the heavy particle temperature at the free-fall edge to the anode surface temperature, has a marked effect on the temperature distribution in the boundary layer. The lower the heavy particle temperature at the free-fall edge, the steeper the temperature gradients for both electrons and heavy particles in the boundary layer. Fig. 4 shows the distribution of electron number density at different values of  $\theta$ . It has a same trend as the temperature distribution because of the strong dependence of electron number density on electron temperature.

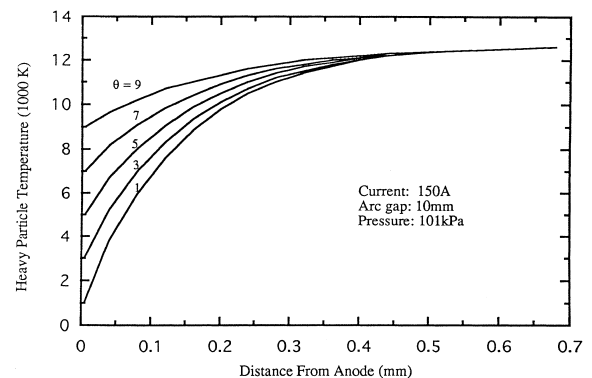


Fig. 2. Distribution of  $T_h$  in the anode boundary layer.

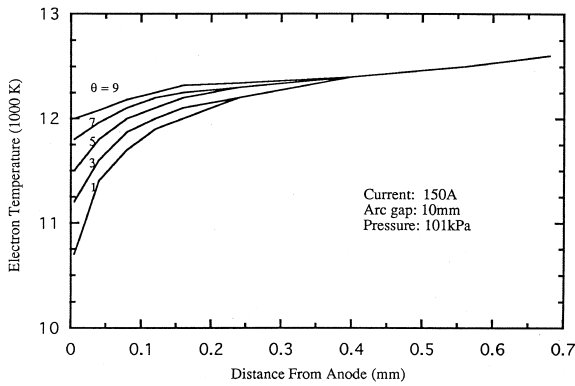


Fig. 3. Distribution of  $T_e$  in the anode boundary layer.

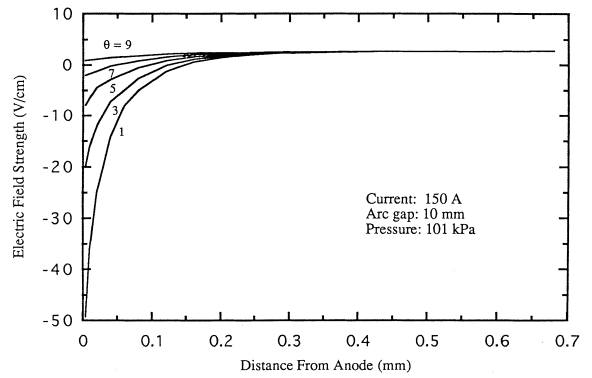


Fig. 5. Electric field distribution in the anode boundary layer.

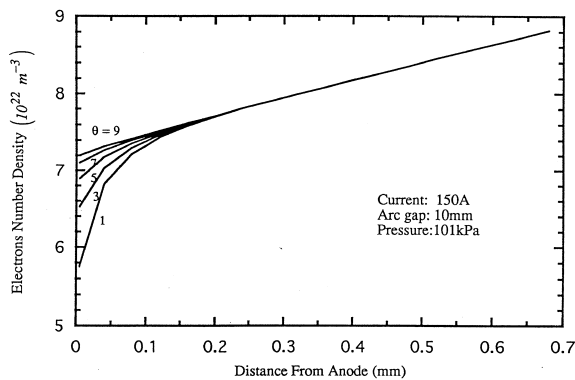


Fig. 4. Distribution of  $n_e$  in the anode boundary layer.

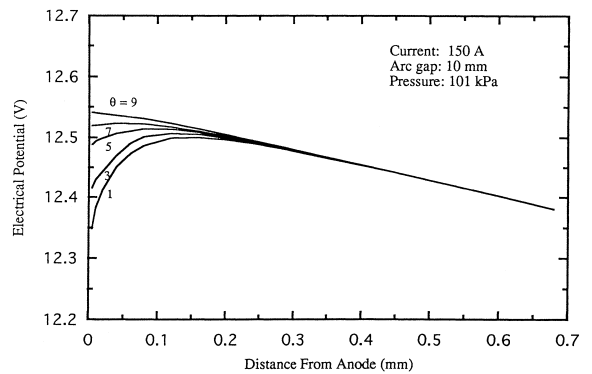


Fig. 6. Electrical potential distribution in the anode boundary layer.

Shown in Figs. 5 and 6 are the electric field strength and the electrical potential in the boundary layer. The electric field strength at the free-fall edge changes from  $8.42 \times 10$  V/m to  $-4.93 \times 10^3$  V/m when  $\theta$  varies from 9 to 1. This fact means that steeper gradients of temperature and electron number density cause an increase of the electric field strength resulted from diffusion in the boundary layer. When  $\theta$  equals to 9, the electric field keeps positive in the whole boundary layer and the electrical potential increases toward the free-fall edge. With decreasing of the heavy particle temperatures at the free-fall edge, the electric field, starting from a small positive value, turns negative at some point inside the boundary layer and reach large negative values at the free-fall edge. Correspondingly, the electrical potential

changes from a slight increase to a decrease as approaching the free-fall edge.

Table 1 demonstrates the influence of the parameter  $\theta$  on plasma scale lengths and potential drop in the boundary layer. The boundary layer thickness  $L_a$ , the electron mean-free-path  $\lambda_e$ , the Debye length  $\lambda_D$ , and the potential drop  $\phi_{i_c} - \phi_{L_a}$  in the boundary layer are all computed from the solution of the governing equations of the anode boundary layer. The results indicate that the boundary layer thickness decreases as the value of  $\theta$  increases. A bigger value of  $\theta$  results in smaller temperature gradients for electrons and ions, which make the deviation between the electron temperature and the heavy particle temperature emerge at a point nearer the free-fall edge so that the boundary layer thickness decreases. The

Table 1

The influence of the ratio  $\theta = T_{hb}/T_a$  on plasma scale lengths and potential drop in the anode boundary layer (current: 150 A, arc gap: 10 mm, pressure: 101 kPa)

$\theta$	$L_a$ (mm)	$\lambda_c$ (mm)	$\lambda_D$ (mm)	$\phi_{i_c} - \phi_{L_a}$ (V)
1	0.287	$0.237 \times 10^{-2}$	$0.298 \times 10^{-4}$	-0.134
3	0.266	$0.238 \times 10^{-2}$	$0.286 \times 10^{-4}$	-0.068
5	0.247	$0.225 \times 10^{-2}$	$0.282 \times 10^{-4}$	0.004
7	0.235	$0.224 \times 10^{-2}$	$0.281 \times 10^{-4}$	0.038
9	0.161	$0.223 \times 10^{-2}$	$0.280 \times 10^{-4}$	0.056

computed results show that the boundary layer thickness is two orders of magnitude larger than the Debye length. With decreasing of the value of  $\theta$ , the potential drop in the boundary layer varies from a slightly positive to a slightly negative.

It is quite evident that the parameter  $\theta$  has great influences on the local plasma properties in the boundary layer and the boundary layer thickness. With the same boundary conditions at the arc column side, the values of heavy particles temperature at the free-fall edge play an important role in determining the key variables in the boundary layer. Up to now, the heavy particle temperature very close to the anode surface is still unclear. Some analyses are restricted to the case of cold ions [12]. Some researchers considered the finite temperature of the ions [13]. But there are no concrete and definite values of the ion temperature in the vicinity of the anode. Therefore, it is necessary to make an estimate of the heavy particle temperature at the free-fall edge. The expression for the heat flux at the anode surface may be written as:

$$\begin{aligned}
 q_a &= q_{ce} + q_{ch} + q_e \\
 &= \left( k_e \frac{dT_e}{dx} \right)_b + \left( k_h \frac{dT_h}{dx} \right)_b \\
 &\quad + J_a \left( 3.203 \frac{k_B}{e} T_{eb} + \phi_w \right),
 \end{aligned} \tag{15}$$

where  $q_a$  the total heat transfer to the anode,  $q_{ce}$  the heat transfer by electron conduction,  $q_{ch}$  the heat transfer by heavy particle conduction,  $q_e$  the heat transfer due to electron flow, and  $\phi_w$  is the work function of the anode material. The subscript b represents the location of the free-fall edge. In general, conduction and convection are not easily separated, i.e., convection modifies the

temperatures gradient at the surface which, in turn, determines the conduction heat transfer to the surface. In this analysis, contributions of conduction and convection are considered together because they are both sensitive to the temperature

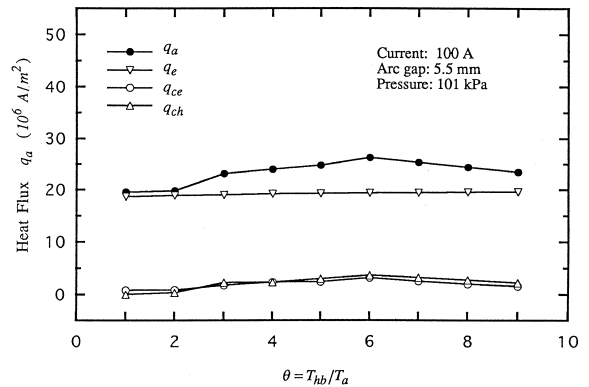


Fig. 7. Heat flux at the anode and its components.

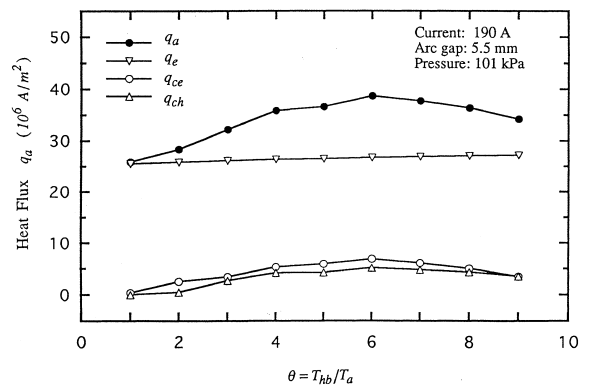


Fig. 8. Heat flux at the anode and its components.

Table 2

Composition of calculated and measured anode maximum heat intensity,  $q_a$ 

Current (A)	Arc gap (mm)	Pressure (kPa)	$\theta$	Calculated, $q_a$ ( $10^6$ A/m <sup>2</sup> )	Measured, $q_a$ ( $10^6$ A/m <sup>2</sup> )
100	5.5	101	6	26.24	27.5
190	5.5	101	6	38.62	40.0

gradients at the free-fall edge. The contribution of plasma radiation to the anode is small [17] and is neglected here. For a rough estimate, the anode fall does not appear in Eq. (15).

Figs. 7 and 8 illustrate the heat flux at the anode as a function of parameter  $\theta$ , for two levels of arc current. In both cases, the term  $q_e$  keeps almost constant because of the dominant effect of arc current on it. For terms  $q_{ce}$  and  $q_{ch}$ , with increasing  $\theta$ , they first go up and then fall slightly. This is because they are determined by both the thermal conductivity and the temperature gradient. When  $\theta$  is small, the temperature gradients for the electron and the ion at the free-fall edge is big, but their thermal conductivity at the location are very low because their temperatures are also low in a case of small  $\theta$ . When  $\theta$  goes up to some value, the temperature gradients get lower, but the variation rate of thermal conductivity does not increase so quickly as in the case of lower  $\theta$ . Thus, the terms  $q_{ce}$  and  $q_{ch}$  decrease slightly in the case of bigger  $\theta$ . Due to the contributions of  $q_{ce}$ ,  $q_{ch}$  and  $q_e$ , the total heat flux at the anode shows the same trend as  $q_{ce}$  and  $q_{ch}$ . In Table 2, a comparison is made for the calculated heat flux at the anode and the measured results of [18]. It shows that if  $\theta$  is equal to six, i.e., the heavy particle temperature at the free-fall edge takes a value of 6000 K, the calculated results agree well with the experimental measurements.

#### 4. Conclusions

A self-consistent model is established for analyzing the physical behavior of the anode region in a high-intensity, atmospheric pressure free-burning argon arc. The boundary conditions for modeling the anode region are taken from the solutions of the flow-affected LTE plasma. Based on the

results of this study the following conclusions may be drawn:

1. The ratio of the heavy particle temperature at the free-fall edge to the anode surface temperature has a great influence on the local plasma properties in the boundary layer, the boundary layer thickness and the sheath potential. The results show that this ratio is around six.
2. The thickness of the anode boundary layer is found to be approximately 0.24 mm for 150 A arcs at an arc length of 10 mm. It is two orders of magnitude larger than the electron mean-free-path which, in turn, is two orders of magnitude large than the Debye length.
3. The potential drop in the anode boundary layer is slightly positive.

#### Acknowledgements

One of the author (C.S. Wu) would like to express his gratitude to the NSF of China for the financial support under the grant No. 59875053.

#### References

- [1] M.I. Boulos, P. Fauchais, E. Pfender, Thermal Plasmas, Plenum Press, New York, vol. 1, 1994, pp. 6–43.
- [2] K.C. Hsu, K. Etemadi, E. Pfender, J. Appl. Phys 54 (1983) 1293–1301.
- [3] O.H. Nestor, J. Appl. Phys 33 (1962) 1638–1648.
- [4] A.E. Guile, M.A. Hilton, I.A. McLelland, J. Phys. D: Appl. Phys 8 (1975) 964–970.
- [5] R.S. Devoto, Phys. Fluids 10 (1967) 2105–2112.
- [6] A.D. Morris, W.C. Gore, Weld. J., 1956, pp. 137–144.
- [7] C.J. Allum, Weld. Met. Fabr 50 (1982) 124–132.
- [8] N.A. Sanders, E. Pfender, J. Appl. Phys 55 (1984) 714–722.
- [9] N.A. Nemchinsky, L.N. Peretts, Zh. Tekh. Fiz 10 (1977) 1868–1875.
- [10] T.K. Bose, Plasma Chem. Plasma Proc 10 (1990) 189–206.
- [11] H.A. Dinulescu, E. Pfender, J. Appl. Phys 51 (1980) 189–206.

- [12] G.A. Emmert, R.M. Wieland, A.T. Mense, J.N. Davidson, *Phys. Fluids* 23 (1980) 803–812.
- [13] I. Senda, *Phys. Plasmas* 2 (1995) 6–13.
- [14] M. Mitchner, C.H. Kruger, Jr., *Partially Ionized Gases*, Wiley, New York, 1973, pp. 146–155.
- [15] C.S. Wu, M. Ushio, M. Tanaka, *Comput. Mater. Sci* 7 (1997) 308–314.
- [16] H.A. Dinulescu: Ph.D. thesis, University of Minnesota, 1979.
- [17] M. Ushio, D. Fan, M. Tanaka, *Trans. JWRI* 22 (1993) 201–207.
- [18] N.S. Tsai, T.W. Eagar, *Metall. Trans* 16B (1985) 841–846.